# A Hybrid FEM-GO Approach to Simulate the NSA in an Anechoic Chamber

**Qian Xu[1], Yi Huang[2], Xu Zhu[2], Lei Xing[1], Paul Duxbury[3] and John Noonan[3]**

[1] College of Electronic and Information Engineering
Nanjing University of Aeronautics and Astronautics, Nanjing, 211106, China
emxu@foxmail.com

[2] Department of Electrical Engineering and Electronics
University of Liverpool, Liverpool, L69 3GJ, United Kingdom
yi.huang@liv.ac.uk

[3] Microwave Vision Group
Haydock, WA 119UY, United Kingdom

***Abstract*** — A hybrid FEM-GO method is proposed and a new CAD tool based on it is developed for anechoic chamber simulation. The proposed method can deal with a chamber with arbitrary shape and arbitrary layout of radio absorbing material. The normalized site attenuation values are simulated and match the measurement results well. It is shown that the proposed method is an efficient and effective way for chamber design and simulation.

***Index Terms*** – anechoic chamber, finite element method, geometric optics, normalized site attenuation.

## I. INTRODUCTION

Anechoic chambers have been widely used for antenna, radar and electromagnetic compatibility (EMC) measurements and tests. There are three key figures of merit to characterize the performance of anechoic chambers: normalized site attenuation (NSA), field uniformity (FU) and site voltage standing wave ratio (SVSWR) [1-2]. Normally, before a chamber is handed over to the customer, an evaluation test from an independent third-part is necessary. If the test fails to pass the required standards/specs, modifications have to be made which is both time consuming and cost ineffective. Thus a prediction of the chamber performance during the design process is needed to ensure a good safety margin to pass the requirements.

However, the design of chambers is difficult and heavily dependent on the designer's experience [3]. The radio absorbing material (RAM) is normally expensive and its size is closely linked to its performance and cost. There is a trade-off between the performance and cost, a better RAM (better absorption rate) normally means more expensive and a larger RAM size. The objective of this paper is to develop an efficient and systematic approach for the anechoic chamber designers to estimate the chamber performance accurately during the design process. The ultimate goal is to minimize the cost (optimize the layout of the RAM) and to maximize the chamber performance.

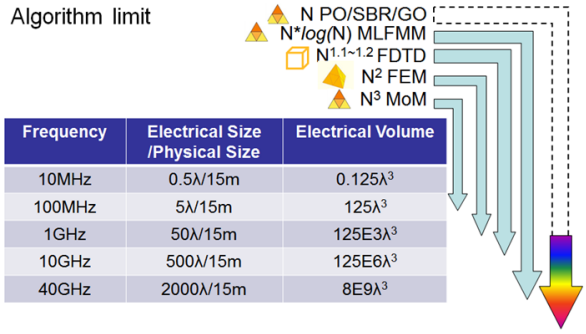


| Frequency | Electrical Size /Physical Size | Electrical Volume |
|---|---|---|
| 10MHz | 0.5λ/15m | 0.125λ³ |
| 100MHz | 5λ/15m | 125λ³ |
| 1GHz | 50λ/15m | 125E3λ³ |
| 10GHz | 500λ/15m | 125E6λ³ |
| 40GHz | 2000λ/15m | 8E9λ³ |

Fig. 1. Comparison of different CEM methods; PO: physical optics, SBR: shooting bouncing ray, GO: geometric optics, MLFMM: multilevel fast multipole algorithm, FDTD: finite-difference time-domain, FEM: finite element method, MoM: method of moment.

A number of computational electromagnetics (CEM) methods have been used for chamber simulation which can be mainly categorized into two classes: full-wave method and high frequency approximation

method. The mesh type, complexity and the electrical size for different methods are summarized in Fig. 1, where *N* means the number of freedoms/unknowns.

For the full-wave method, transmission line matrix (TLM) [4], MoM/FEM (method of moment/finite element method) [5] and FDTD (finite-difference time-domain) [6] have been used to simulate this study. Because the size of chambers is normally electrically large, even with a high performance computer, large electrical size problems with complex material scenarios are not easy to solve due to the required large memory and time consumption. Another issue is, in the full-wave method, the detailed material property distribution (as a function of the frequency and depth) should be known, and the antenna 3D structures need to be defined. In the design process, these details may not be completely available.

For the high frequency approximation method, such as the geometric optics (GO) has been proven to be a fast and efficient way to simulate this problem [7-12]. However, the RAM model directly determines the accuracy of the simulated result. The RAM reflectivity has been characterized by using analytical models which include: a cosine approximation [8], an effective medium [13], a homogenization model [14] and a multi-layer model [9]. Thus, the RAM is not fully described and a simplified analytical model over a wide frequency range and a wide incident angle is normally not available. The complexity of the analytical model also reduces the speed of GO, because the reflected field needs to be calculated using complex equations or an iterative method.

In this paper, we hybridize a full-wave method (FEM) and a high frequency method (GO) to realize a systematic approach for the chamber design. In the micro level, the RAM is analyzed using the FEM. By using the periodical boundary condition (PBC) only one RAM element needs to be analyzed. After the FEM analysis is completed, the reflection coefficients of the RAMs are saved in a database. The GO is used to simulate the whole chamber which is electrically large; the local reflection coefficient will be extracted from the database obtained from the FEM. Thus the FEM and the GO are combined seamlessly. Finally, the simulated results are verified by measurements completed by an independent third party.

## II. THEORY

In this section, the proposed hybrid method is introduced with essential details.

### A. GO

It is well known that in the GO, the electric field is assumed to propagate like light as shown in Fig. 2. At the boundary of different materials, the wave is reflected and transmitted.

The E-field at the field point can be expressed as [15-16]

$$\vec{E} = \vec{E}_0 \cdot \left\{\prod \bar{\bar{R}}_i\right\} \cdot \left\{\prod \bar{\bar{T}}_i\right\} \cdot \left\{\prod e^{-\gamma_i l_i}\right\} \cdot SF. \quad (1)$$

where $A_0$ and $A$ in Fig. 2 are the cross-sectional area of the ray tubes at the source point and field point of interest, they will be used to calculate the spreading factor ($SF = \sqrt{A_0}/\sqrt{A}$). $\vec{E}_0$ is the E-field at the source point (reference point), $\vec{E}$ is the E-field at the field point. $\prod \bar{\bar{R}}_i$ and $\prod \bar{\bar{T}}_i$ are the reflection and transmission coefficient dyads along the whole ray path, $\prod e^{-\gamma_i l_i}$ is the total phase variations and losses along the whole path.

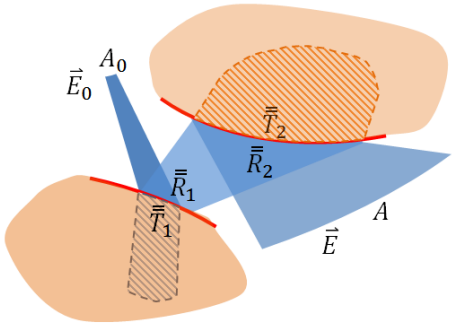


Fig. 2. Wave propagation in GO.

In the anechoic chamber simulation, only reflections are considered. Thus equation (1) can be simplified as

$$\vec{E} = \vec{E}_0 \cdot \left\{\prod \bar{\bar{R}}_i\right\} \cdot \left\{\prod e^{-\gamma_i l_i}\right\} \cdot SF. \quad (2)$$

where $\bar{\bar{R}}$ relates the incident field $\vec{E}^i$ and reflected field $\vec{E}^r$ as

$$\vec{E}^r = \begin{bmatrix} E_\parallel^r \\ E_\perp^r \end{bmatrix} = \bar{\bar{R}} \cdot \vec{E}^i = \begin{bmatrix} R_{\parallel\parallel} & R_{\parallel\perp} \\ R_{\perp\parallel} & R_{\perp\perp} \end{bmatrix} \begin{bmatrix} E_\parallel^i \\ E_\perp^i \end{bmatrix}. \quad (3)$$

where $E_\parallel$ and $E_\perp$ are the decomposed parallel component and perpendicular component of the E-field (Fig. 3).

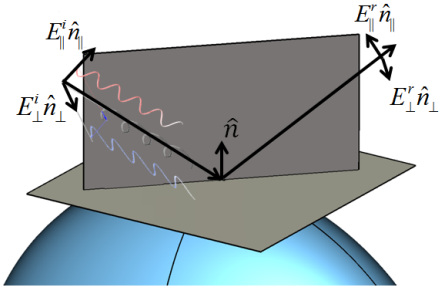


Fig. 3. Decomposed incident and reflected waves.

When the GO is applied to the anechoic chamber scenario, as shown in Fig. 4, the rays between the transmitting (Tx) antenna and the receiving (Rx) antenna need to be found out [17]. Once the routes of the rays are known, the incident angles are known, equation (3) will be used to calculate the reflected field. Finally, the vector superposition is performed at the Rx antenna to calculate the total E-field.

There are issues to be carefully treated. When the ray is launched from the Tx antenna, an initial E-field $\vec{E}_0$ needs to be determined. This requires the radiation pattern of the antenna to be known, we consider the radiation pattern as a function of $(\theta, \varphi)$, then an interpolation is implemented for an arbitrary launching angle.

Another issue is that $\bar{\bar{R}}$ needs to be determined; we may have different RAM types in a chamber. Since the reflection coefficient is a complex number, and it is related to the incident angle, frequency and polarization. It is noted in equation (3), $\bar{\bar{R}}$ includes four elements: $R_{\parallel\parallel}$, $R_{\parallel\perp}$, $R_{\perp\parallel}$ and $R_{\perp\perp}$, they can be considered as a function of incident angle and frequency $R_{ij} = R_{ij}(\theta, \varphi, f)$ ($i$, $j$ can be $\parallel$ or $\perp$). We use a 3D matrix to save each element in the database. In the next section, the FEM is used to obtain the $\bar{\bar{R}}(\theta, \varphi, f)$ for different type of RAM. The workflow is shown in Fig. 5, we use the triangular surface mesh in the model described by .stl file [18].

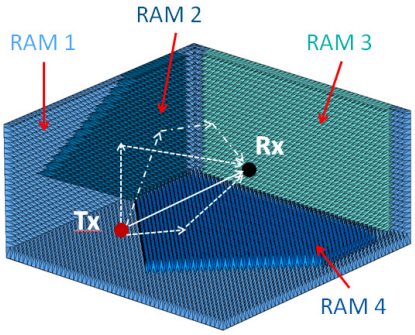


Fig. 4. GO rays in an anechoic chamber with four different types of RAM.

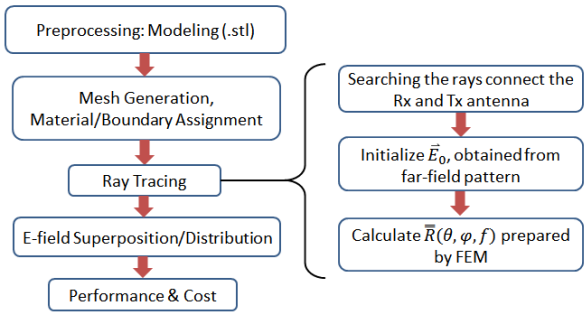


Fig. 5. The workflow of the FEM-GO.

**B. FEM analysis**

The FEM analysis is performed before the rays are launched, and only need to be analyzed once for each material. All the data obtained from the FEM simulation will be saved in a database/matrix which will be used by the GO.

It should be noted that the reflection coefficient $\bar{\bar{R}}$ can be obtained from measurement using the arch method [19]. It can also be obtained from simulation; the simulation model in the FEM is shown in Fig. 6. By applying the PBC, only one unit cell needs to be analyzed [20]. For each incident angle, two orthogonal incident waves/modes need to be analyzed, shown in Fig. 7. Frequency sweep is adopted for each incident angle. When all the simulation/measurements are finished, $\bar{\bar{R}}$ is ready. Since we can only simulate some discrete incident angles, for an arbitrary incident angle, the reflection coefficient can be obtained using interpolation.

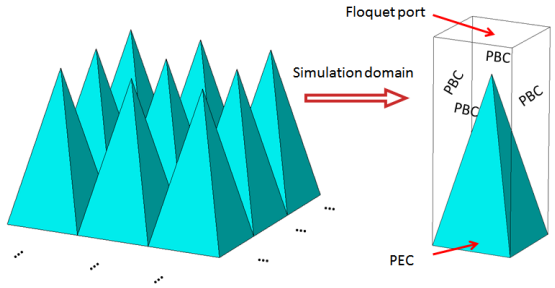


Fig. 6. The simulation model of the pyramid absorber.

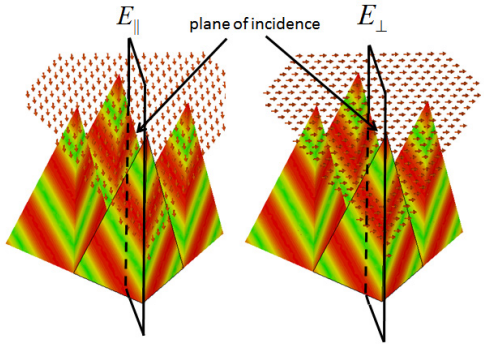


Fig. 7. Two orthogonal incident waves/modes.

A typical value of $\bar{\bar{R}}$ at 3 GHz is shown in Fig. 8 (magnitude) and Fig. 9 (phase) with different incident angles. A 5° step is used for both $\theta$ and $\varphi$ directions, for other values 2D interpolation is used, note that at the edge of the figure (large incident angle) the transition is not very smooth, this is because we have used the nearest available value to interpolate it.

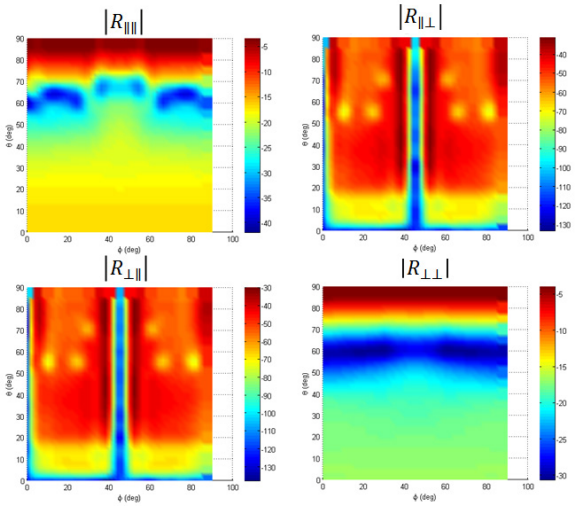


Fig. 8. Typical magnitude values of each element of $\bar{\bar{R}}$, unit: dB.

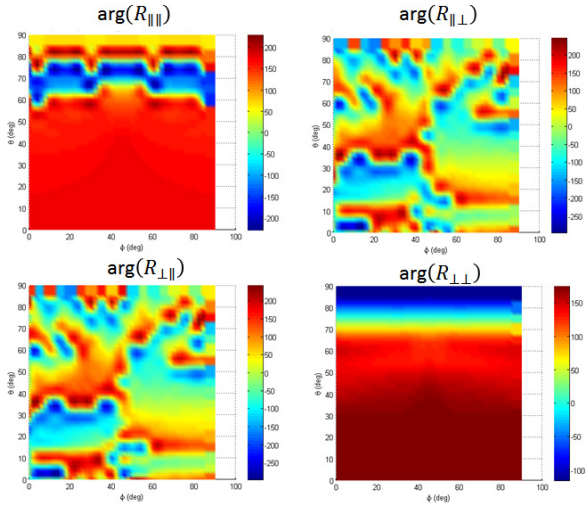


Fig. 9. Typical phase values of each element of $\bar{\bar{R}}$, unit: degree.

### C. NSA definition

After the FEM-GO analysis is finished, the NSA values can be extracted from the E-field distribution. The test scenario is shown in Fig. 10. The measurement distance is can be 3 m, 10 m or 30 m, depending on the relevant standards. The radiation power is assumed to be 1 W and the NSA value can be obtained from [21]

$$NSA_{dB} = 46.76 + Gain(dBi) - 20\log(f) - 20\log(E_{max}). \quad (4)$$

where $f$ is the frequency of interest in MHz, $E_{max}$ is the maximum magnitude of the electric field strength in V/m at the location of receiving antenna by scanning the height from 1 m to 4 m.

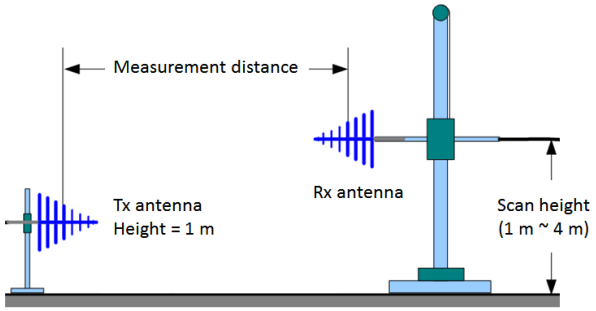


Fig. 10. NSA measurement setup.

## III. SIMULATION AND MEASUREMENTS

The simulation and verification for an ideal chamber has been done and a very good agreement has been obtained in [22]. In this paper, we compare the simulated results and the measured results for a real chamber.

The size of the selected chamber is 9 m × 6 m × 6 m ($L \times W \times$ H). It is shown in Fig. 11(a) which is a semi-anechoic chamber for EMC tests and the simulation model is given in Fig. 11(b). Three different types of RAMs are used which are shown in different colors. Triangular meshes are used to represent the chamber, the mesh number is 70.

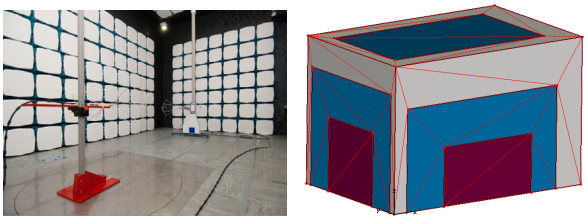

(a) (b)

Fig. 11. (a) Test chamber and (b) the simulation model.

The test scenarios are shown in Fig. 12 and listed in Table 1. Four different locations of the Rx antenna in the turntable region are tested: left (L), right (R), front (F) and center (C). At each location, there are two height values and two polarizations for the Tx antenna. These makes 2 × 2 × 4 = 16 cases in total.

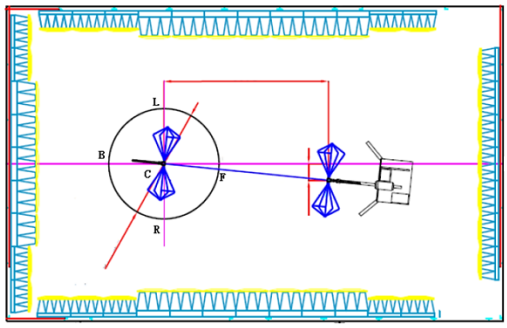


Fig. 12. Test scenarios with Tx and Rx antenna.

Table 1: NSA test scenarios

| Polarization | Height | Tx Position |
|---|---|---|
| Horizontal (H) | Lower (L) | Center (C)<br>Front (F) |
| Vertical (V) | Upper (U) | Right (R)<br>Left (L) |

The simulation time for each scenario is around 2 minutes on a standard personal computer; the memory consumption is around 600 MB. The rays between the Tx and Rx (two height values) antennas are shown in Fig. 13.

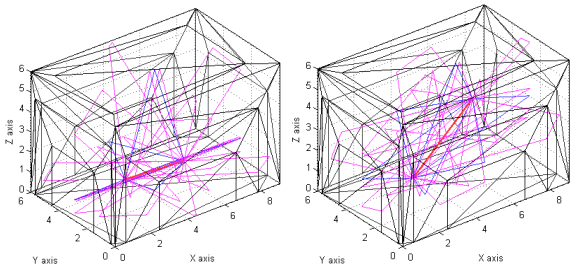


Fig. 13. (a) Rx antenna height is 1 m; (b) Rx antenna height is 4 m.

A typical result is shown in Fig. 14, the limit in the CISPR standard [1] is also given in the same figure. As can be seen, they are in a very good agreement. We have also compared the NSA values of all 16 cases, all the errors are in the range of $\pm 2$ dB.

## IV. CONCLUSION

A systematic approach has been proposed in this paper for anechoic chamber performance prediction and analysis, which combines both the full-wave method (FEM) and the high frequency approximation method (GO). It has been shown that the proposed method is efficient and accurate for the anechoic chamber simulation and suitable for real work chamber design. The results from simulation and measurement show that the error was smaller than $\pm 2$ dB over the whole frequency range.

It should be noted that although GO is very fast, prepared data from the FEM is needed. To obtain $\bar{\bar{R}}$ at different incident angle, polarization, frequency is time consuming. However, this kind of simulation/arch measurement needs to be done only once. After it is finished the data can be reused, which saves much computing time compared with other methods.

Future work may include more detailed research on different kinds of chambers (e.g. tapered, compact chambers) and the limitation of the hybrid method.

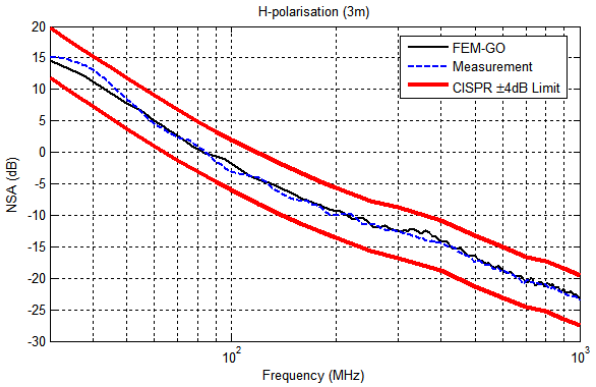


(a)

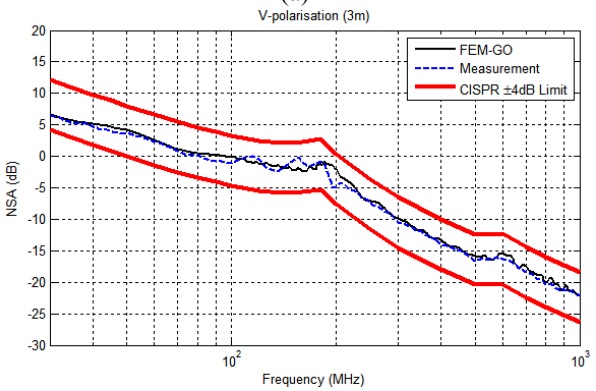


(b)

Fig. 14. Simulated and measured NSA values for the lower height, left Tx antenna position in Table 1. (a) horizontal polarization; (b) vertical polarization.

## ACKNOWLEDGMENT

This project was supported in part by the Center for Global Eco-Innovation with project No. 139 and MVG (Microwave Vision Group), National Natural Science Foundation of China (61701224 and 61601219) and Nature Science Foundation of Jiangsu Province (BK20160804).

## REFERENCES

[1] CISPR 16-1-4: *Specification for radio disturbance and immunity measuring apparatus and methods - Part 1-4: Radio disturbance and immunity measuring apparatus - Antennas and test sites for radiated disturbance measurements*, IEC Standard, Ed 3.1, Jul. 2012.

[2] IEC 61000-4-3: *Electromagnetic compatibility (EMC) - Part 4-3: Testing and measurement techniques - Radiated, radio-frequency, electromagnetic field immunity test*, IEC Standard, Ed 3.1, Apr. 2008.

[3] L. H. Hemming, *Electromagnetic Anechoic Chambers: A Fundamental Design and Specification Guide*, New York: Wiley-IEEE Press, 2002.

[4] Available:*https://www.cst.com/Applications/Article/Intelligent-Representation-Of-Anechoic-Chamber-Wall-Cuts-Electromagnetic-Simulation-Time-95*.
[5] D. Campbell, G. Gampala, C. J. Reddy, M. Winebrand and J. Aubin, "Modeling and analysis of anechoic chamber using CEM tools," in *Proceedings of AMTA Conference*, Bellevue, 2012.
[6] N. V. Kantartzis and T. D. Tsiboukis, "Wideband numerical modelling and performance optimisation of arbitrarily-shaped anechoic chambers via an unconditionally stable time-domain technique," *Electrical Engineering*, vol. 88, iss. 1, pp. 55-81, Nov. 2005.
[7] B. K. Chung, C. H. The and H. T. Chuah, "Modeling of anechoic chamber using a beam-tracing technique," *Progress In Electromagnetics Research (PIER)*, vol. 49, pp. 23-38, 2004.
[8] S. R. Mishra and T. J. F. Pavlasek, "Design of absorber-lined chamber for EMC measurements using a geometrical optics approach*," IEEE Trans. Electromagnetic Compatibility*, vol. EMC-26, no. 3, pp. 111-119, Aug. 1984.
[9] M. K. Mansour and J. Jarem, "Anechoic chamber design using ray tracing and theory of images," in *IEEE Southeastcon '90 Proceedings*, New Orleans, 1990, pp. 689-695.
[10] C. L. Holloway and E. F. Kuester, "Modeling semi-anechoic electromagnetic measurement chambers," *IEEE Trans. Electromagnetic Compatibility*, vol. 38, no. 1, pp. 79-94, Feb. 1996.
[11] M. Lin, J. Ji, C. G. Hsu and H. Hsieh, "Simulation and analysis of EMC chambers by ray tracing method," in *IEEE International Symposium on Electromagnetic Compatibility*, Honolulu, 2007, pp. 1-4.
[12] S. M. J. Razavi, M. Khalaj-Amirhosseini and A. Cheldavi, "Minimum usage of ferrite tiles in anechoic chambers," *Progress In Electromagnetics Research B (PIER B)*, vol. 19, pp. 367-383, 2010.
[13] B. K. Chung, H. T. Chuah, "Modeling of RF absorber for application in the design of anechoic chamber," *Progress In Electromagnetics Research, (PIER)*, vol. 43, pp. 273-285, 2003.
[14] E. F. Kuester and C. L. Holloway, "A low-frequency model for wedge or pyramid absorber arrays-I: theory," *IEEE Trans. Electromagnetic Compatibility*, vol. 36, no. 4, pp. 300-306, Nov. 1994.
[15] C. A. Balanis, *Advanced Engineering Electromagnetics*, John Wiley & Sons, 1989.
[16] C. Yang, B. Wu and C. Ko "A ray-tracing method for modeling indoor wave propagation and penetration," *IEEE Trans. Antennas Propagat.*, vol. 46, no. 6, pp. 907–919, Jun. 1998.
[17] C. Saeidi, A. Fard and F. Hodjatkashani, "Full three-dimensional radio wave propagation prediction model," IEEE Trans. Antennas Propagat., vol. 60, no. 5, pp. 2462–2471, May 2012.
[18] M. Bruns, Automated Fabrication: *Improving Productivity in Manufacturing*, Prentice Hall, 1993.
[19] IEEE Std 1128-1998: *IEEE Recommended Practice for Radio-Frequency (RF) Absorber Evaluation in the Range of 30 MHz to 5 GHz*, IEEE Standard, Apr. 1998.
[20] J. Jin, *The Finite Element Method in Electromagnetics*, Wiley, 3rd Ed., 2014.
[21] V. P. Kodali, *Engineering Electromagnetic Compatibility: Principles, Measurements, Technologies, and Computer Models*, 2nd Ed, New York: Wiley-IEEE Press, 2001
[22] Q. Xu, Y. Huang, X. Zhu, L. Xing, P. Duxbury and J. Noonan, "NSA simulation in semi-anechoic chamber using ray tube tracing method," *9th IET International Conference on Computation in Electromagnetics (CEM 2014),* , London, UK, March, 2014.

**Qian Xu** received the B.Eng. and M.Eng. degrees from the Department of Electronics and Information, Northwestern Polytechnical University, Xi'an, China, in 2007 and 2010, respectively, and the Ph.D. degree in electrical engineering from the University of Liverpool, Liverpool, U.K., in 2016.

He was an RF Engineer in Nanjing, China, in 2011, an Application Engineer with CST Company, Shanghai, China, in 2012, and a Research Assistant with the University of Liverpool, in 2016. He is currently an Associate Professor in College of Electronic and Information Engineering, Nanjing University of Aeronautics and Astronautics, Nanjing, China. His current research interests include anechoic chamber, reverberation chamber, computational electromagnetics and statistical electromagnetics.

**Yi Huang** received the B.Sc. degree in physics from Wuhan University, Wuhan, China, in 1984, the M.Sc.(Eng.) degree in microwave engineering from the Nanjing Research Institute of Electronics Technology (NRIET), Nanjing, China, in 1987, and the D.Phil. degree in communications from the University of Oxford, Oxford, U.K., in 1994.

He was a Radar Engineer with the NRIET, and a Member of Research Staff with the University of

Birmingham, Birmingham, U.K., the University of Oxford, Oxford, U.K., and the University of Essex, Colchester, U.K. He was a Research Fellow with the British Telecom Laboratories in 1994, and then with the Department of Electrical Engineering & Electronics, University of Liverpool, Liverpool, U.K., as a Faculty Member, in 1995, where he is currently a Full Professor of Wireless Engineering, the Head of High Frequency Engineering Research Group, M.Sc. Program Director, and the Deputy Head of Department. He has authored over 200 refereed papers in leading international journals and conference proceedings, and is the Principal Author of the popular book Antennas: from Theory to Practice (Wiley, 2008). He has received many research grants from research councils, government agencies, charity, EU, and industry, acted as a Consultant to various companies, and served on a number of national and international technical committees. His current research interests include wireless communications, applied electromagnetics, radar, and antennas.

Prof. Huang is a Fellow of the IET. He has been an Editor, and an Associate Editor or a Guest Editor of four of international journals. He has been a keynote/invited speaker and organizer of many conferences and workshops (e.g., IEEE iWAT 2010, WiCom 2006, 2010, and LAPC2012). He is currently the Editor-in-Chief of Wireless Engineering and Technology, Associate Editor of the IEEE Antennas and Wireless Propagation Letters, and a U.K. and Ireland Rep to the European Association of Antennas and Propagation.